Membrane Orientation and Lateral Diffusion of BODIPY-Cholesterol as a Function of Probe Structure

Lukasz M. Solanko, [†] Alf Honigmann,[¶] Henrik Skov Midtiby, [‡§] Frederik W. Lund, [†] Jonathan R. Brewer, [†‡] Vjekoslav Dekaris,[‖] Robert Bittman,[‖] Christian Eggeling [¶**] and Daniel Wüstner [†*]

[†]Department of Biochemistry and Molecular Biology and [‡]MEMPHYS Center for Biomembrane Physics, Department of Pharmacy, Chemistry and Physics and [§]Institute for Chemical, Biological and Environmental Technology, University of Southern Denmark, DK-5230 Odense M, Denmark, [¶]Max Planck Institute for Biophysical Chemistry, Dept. of NanoBiophotonics, Am Fassberg 11, 37077, Göttingen, Germany, [‖]Department of Chemistry and Biochemistry, Queens College, The City University of New York, Flushing, NY 11367, USA, **Human Immunology Unit, Weatherall Institute of Molecular Medicine, University of Oxford, Oxford OX3 9DU, United Kingdom

Supporting Material

Preparation of SUVs, LUVs, and GUVs

a) SUVs and LUVs: To assess the fluorescence properties of B-P-Chol, SUVs were prepared from POPC and varying amounts of the fluorescent sterols dissolved in chloroform and ethanol, respectively. After evaporation of the solvents under a stream of nitrogen, PBS was added to the lipid film, giving a total lipid concentration of 31 μM. The lipid suspension was vortexed and afterwards sonicated using a Branson sonicator to obtain SUVs as described (1). To assess the effect of membrane curvature on fluorescence properties, we performed the same experiment with LUVs made by extrusion using a MicroExtruder (Avanti Polar Lipids, Alabaster, AL).

b) GUVs: For partition experiments, GUVs were prepared from DPPC, DOPC and cholesterol in mol percentages of 33:33:33 together with 0.5 mol% DiIC12 and 0.5 mol% of either B-Chol or B-P-Chol as described previously (1).

For polarization experiments, GUVs were prepared from 69:30 mol% POPC and cholesterol, with either 1 mol% B-Chol or B-P-Chol. Lipids were mixed in chloroform to a final total lipid concentration of 0.25 mM, from which 4 μl were deposited onto the platinum wires in the Teflon electroformation chamber. GUV electroformation was carried out over 2 h with an applied AC field with 670 V/m amplitude and 10 Hz frequency (2). For all lipid compositions, the temperature during electroformation was above the main phase transition of each phospholipid to prevent gel domain formation in the GUVs.

Preparation of supported lipid bilayers (SLBs)

SLB were prepared by spin-coating (2000 rpm) the lipid solution (2 g/l) in methanol and chloroform (1:1) on piranha-cleaned cover glass. After evaporation of the solvents under vacuum for 30 min, the membrane was hydrated with 150 mM NaCl, 10 mM Tris/HCl buffer, pH 7.5, and

rinsed with that buffer until a single clean bilayer remained. Fluorescent probes were added to the lipid solution at a final concentration of 0.01 mol%.

Fluorescence excitation and emission spectroscopy

Emission spectra of B-P-Chol in LUVs and SUVs were recorded using an ISS Chronos spectrofluorometer (ISS, Champaign, IL). The spectrofluorometer was equipped with exchangeable LED light sources for excitation, and an LED emitting light of 480 nm +/- 10 nm was used for exciting the BODIPY sterol probes. In the excitation path, a slit with 2 mm width was mounted. The emission maximum at 508 nm was plotted as a function of sterol mole fraction. The initial concentration at which B-P-Chol began to self-quench was determined, exactly as in previous measurements for B-Chol (1). Absorption spectra were recorded on a Perkin Elmer Lambda 35 spectrophotometer.

Cell culture and labelling

Fetal bovine serum (FBS) and DMEM were obtained from Gibco BRL (Life Technologies, Paisley, Scotland), if not stated otherwise. Buffer medium contained 150 mM NaCl, 5 mM KCl, 1 mM $CaCl_2$, 1 mM $MgCl_2$, 5 mM glucose, and 20 mM HEPES, pH 7.4. Baby hamster kidney (BHK) cells were grown in DMEM supplemented with 10% heat-inactivated FBS and 2 mM L-glutamine, 100 units/ml penicillin, 100 µg/ml streptomycin, 0.4 mg/ml geneticin, 0.2 µg/ml puromycin, and 1 µg/ml tetracycline. Two to three days prior to experiments, cells were seeded on microscope slide dishes coated with poly-D-lysine. Kidney epithelial cells (*Cercopithecus aethiops,* Veros) were cultured under constant conditions at 37°C and 5% CO_2 in DMEM (Invitrogen, Carlsbad, CA) containing 5% FBS (PAA, Pasching, Austria), 100 units per ml streptomycin, 100 µg/ml penicillin (all from Biochrom, Berlin, Germany), and 1 mM pyruvate (Sigma, St.Louis, MO). Fluorescent probes were stored in ethanol at a concentration of 5 mM under nitrogen at – 80°C until use. B-Chol and B-P-Chol were loaded onto methyl-β-cyclodextrin (CD) including fatty acid free bovine serum albumin (BSA) as described previously (12), giving a solution containing complexes of B-Chol/cyclodextrin (B-Chol-CD) and B-P-Chol/cyclodextrin (B-P-Chol-CD), respectively. Cells were labeled with B-Chol-CD or B-P-Chol for 1 min at 37°C, washed, and chased for 5 min, 30 min, or 60 min in buffer medium at 37°C prior to imaging.

Multicolor wide field microscopy

For co-detection of DiIC12 and BODIPY-tagged cholesterol analogs in GUVs, wide-field fluorescence microscopy and digital image acquisition were performed with a Leica DMIRBE microscope equipped with a 63x, 1.4 NA oil immersion objective (Leica Lasertechnik, Wetzlar, Germany) and an electron-multiplication Andor Ixon^{EM} blue CCD camera driven by the Solis software supplied with the camera. DiIC12 was imaged using a standard rhodamine filter set [535-nm (50-nm bandpass) excitation filter, 565-nm dichromatic mirror, and 610-nm (75-nm) bandpass) emission filter]. BODIPY-tagged cholesterol analogs were imaged using a standard fluorescein filter set [470-nm, (20-nm bandpass) excitation filter, 510-nm dichromatic mirror, and 537-nm (23-nm) bandpass) emission filter].

Two-photon excitation microscopy

Fluorescence polarization and time lapse measurements of BODIPY-tagged sterols were performed using a custom-built setup constructed around an Olympus IX70 microscope. The objective used was a 60x water immersion objective with a NA of 1.2. The excitation light source was a femtosecond Ti:Sa laser (Broadband Mai Tai XF W25 with a 10 W Millennia pump laser, 80 MHz pulse-frequency, tuneable excitation range 710-980 nm, Spectra Physics, Mountain View, CA) and the excitation wavelength used was 930 nm. For fluorescence polarization and time-lapse imaging, linear and circular polarized excitation light was used, respectively. Polarization measurements were performed by clock-wise motorized rotation of a λ half wave plate at 5^o angles giving a 10^o rotation of the incident electric field vector, ***E*** (3). One measurement consisted of acquiring 36 frames corresponding to one full rotation of the incident ***E***-vector with a count rate of 10^2 to 10^3 lasting in total for about 1 min at our set-up. For highly asymmetric dye molecules, the two-photon fluorescence emission varies as ~ $\cos^4$ to the angle between ***E*** and the electronic transition moment of the fluorophore, ***p***. For that reason, one can determine the orientation of the fluorescent group by mapping the angular intensity variation as function of the orientation of the incident electric field ***E*** (3). For a quantitative analysis, measured fluorescence must be corrected for angle variations of the emission intensity not originating from the probe response, since we found that the transmission of excitation and emission light through the optical train of the microscope depends slightly on polarization angle (3). Therefore, we performed not only measurements with both BODIPY-cholesterol probes in model and cell membranes but also with the B-Chol-CD and B-P-Chol-CD solutions. In the latter case, the fluorophore orientation is isotropic and any intensity variations are a direct measure of the instrument response. Images stacks of model and cell membranes containing the BODIPY-tagged sterols were, therefore, divided by the stacks acquired for the fluorophore solutions after adding one integer value to the latter images to avoid division by zero in all pixel positions. This also corrected for shading, i.e. spatially varying brightness differences over the image field. Afterwards, angle variations were analyzed in terms of the discrete Fourier transform of the pixel intensities as described below. To collect emission of the two BODIPY-tagged cholesterol probes, a 540 ± 25 nm filter was used (BrightLine HC). The light was detected by a photomultiplier tube (Hamamatsu H7422P-40) operated in photon-counting mode. The data were acquired using simFCS software developed by the Laboratory for Fluorescence Dynamics (University of California, Irvine, CA).

Image analysis for polarization measurements

The angle variations of fluorescence detected absorption anisotropy were analyzed by means of a discrete Fourier transform of the pixel intensities. The intensity variation of a single pixel is denoted by $I^{xy}_n(n\Delta\phi)$ where n is an integer. The complex valued discrete Fourier transform of the pixel with indices x and y is then given by:

$$\widetilde{I}^{xy}_{\gamma} = \frac{1}{N}\sum_{n=0}^{N-1} I^{xy}_{n} \cdot \exp\left(-i \cdot 2\pi \cdot \frac{\gamma \cdot n}{N}\right) \qquad \text{(S1)}$$

Here, N = 36 corresponding to the number of frames acquired every 10° for a full rotation of 360°. A $\cos^4 \phi$ intensity dependence will have a periodicity of 180° and the component $\hat{I}^{xy}_2$ will dominate with $\hat{I}^{xy}_4$ as a smaller overtone. It is sufficient to consider the principal one $\hat{I}^{xy}_2$ since the relative magnitude of these two Fourier components is constant for a $\cos^4$ dependence. The argument ½ arg($\hat{I}^{xy}_2$) depict the orientation angle of the BODIPY dipole within a given pixel. The modulus $|\hat{I}^{xy}_2|$ is a measure of the degree of orientation corresponding to the length of the molecular director **c**. The Fourier analysis using $\gamma = 2$ was performed at the single pixel level, generating a spatial map of the orientation and magnitude of the molecular director **c** (see Fig. S2D for a definition of **c**). These routines were written in MatLab (Mathworks, USA); for details, see (3). For spatial registration of image stacks, we used "StackReg" (developed by Dr. Thevenaz at the Biomedical Imaging group, EPFL, Lausanne, Switzerland) and for the image analysis we used ImageJ (developed at the U.S. National Institutes of Health and available on the Internet at http://rsb.info.nih.gov/ij) (4). Intensity profiles were measured in ImageJ and plotted in SigmaPlot 9.0 (SPSS Inc, Chicago, IL). For image visualization, ImageJ and Adobe Photoshop were used.

FRAP

FRAP experiments were performed on a Zeiss LSM510 confocal microscope. The microscope was focused on the plasma membrane on top of the cells with a pinhole size of 1 airy unit. Here a circular region of interest (ROI) with a radius, r, of 1.8 or 2.8 µm was bleached, and the fluorescence recovery was imaged over 45 frames with a laser intensity of 0.2%. This low laser power prevented significant photobleaching during image recording, as we verified in control experiments. To increase the image acquisition speed, we zoomed in on a square area with a side length of $2r$, where r is the radius of the ROI. Thus, for a ROI with radius r = 1.8 µm and r = 2.8 µm, images were acquired with a frame rate of 1.7 and 1.3 frames per sec, respectively. The fluorescence recovery curve for each image sequence was measured by determining the integrated intensity for the selected ROI (I_{ROI}) and separately for the whole cell (I_{cell}). By dividing I_{ROI} by I_{cell}, we could correct for the low photobleaching as well as for occasional small focus drifts during image recording. This is verified for the case of photobleaching in simulated FRAP experiments, as outlined below (see Fig. S7). Subsequently, the whole sequence was normalized by dividing through the prebleach intensity $F_{pre} = I_{ROI}(t=0)/I_{cell}(t=0)$, and the final recovery curve for each experiment was given by the mean of five recovery curves. To determine the lateral diffusion coefficient, one needs first the half-time of recovery (5, 6), which we determined by fitting the recovery curves to:

$$F(t) = A \cdot \left(1 - \exp(-k \cdot t)\right) + F(0) \quad \text{, with} \quad A = F(\infty) - F(0) \qquad \text{(S2a, b)}$$

Here, $F(0)$ is the fluorescence intensity at time t = 0 (i.e., immediately after bleaching), $F(\infty)$ is the final fluorescence intensity at the end of the recovery phase, and $t_{½} = \ln 2/k$ is the half time of recovery. From this the lateral diffusion constant is given by (6):

$$D = \frac{\beta r^2}{4 t_{½}}, \qquad \text{(S3)}$$

, where r is the radius of the ROI and β is a constant determined by the percentage of bleach. Here the percentage of bleach was ~55%, for which $\beta = 1.18$ (6).

FCS

FCS was performed on a home-built confocal microscope. For excitation of BODIPY, a blue laser diode (485 nm, 4μW, ≈ 80 ps pulse width, LDH-P-485B, PicoQuant) was coupled into an oil immersion objective (HCXPLAPO NA = 1.4, Leica Microsystems). Precise positioning of the laser focus in the sample and sample scanning was realized by a digital beam scanning unit (Yanus, Till-Photonics, Gräfeling, Germany) for lateral directions and a piezo scanning stage (NanoMax-TS Stage, Thorlabs, Newton, MA) for the axial direction. The fluorescence was descanned and coupled into a multi-mode fiber splitter (Fiber Optic Network Technology, Surrey, Canada) with an aperture size corresponding to 1.4× the magnified excitation spot. The fluorescence signal was then detected by single-photon counting modules (avalanche photodiode SPCM-AQR-13-FC, Perkin Elmer Optoelectronics), and the collected fluorescence counts were recorded by a single-photon counting PCI card (Becker & Hickl) or an USB correlator card (Flex02-01D, Correlator.com). Details of the FCS analysis are outlined in (7, 8). The correlation data were fitted to:

$$G(t_c) = \frac{1}{N} \cdot \left(1 + \frac{p}{(1-p)}\right) \cdot \exp\left(-\frac{t_c}{t_T}\right) \cdot \frac{1}{1 + \left(\frac{t_c}{\tau_D}\right)^{\alpha}} \qquad \text{(S4)}$$

, where N is the particle number (i.e., the mean number of fluorescent molecules in the detection volume), which is proportional to the concentration divided by the measurement volume (or area for two-dimensional samples), p is the fraction of dye that is on average in the dark triplet state, t_T is the triplet correlation time, τ_D is the average transit time of the fluorescent molecules diffusing through the observation area, and α is the anomaly exponent, which is 1 if the diffusion is free and <1 for anomalous hindered diffusion. All FCS measurements were performed at the lower, surface attached part of the PM.

STED-FCS

Sub-diffraction observation spots were obtained using STED-microscopy (22). BODIPY fluorescence was depleted with a 577 nm continuous-wave optically pumped semiconductor laser (Coherent). The doughnut-shaped focal intensity distributions of the STED beam featuring a central zero was produced by introducing a phase-modifying plate (RPC Photonics) into the beam path, imprinting a helical phase ramp ($\exp(i\varphi)$ with $0 \leq \varphi \leq 2\pi$) onto the wave front. A λ/4-plate ensured circular polarization of the STED and of the excitation beam. The maximum laser power in the objective was ~80 mW for the 577 nm STED and 4 μW for the 485nm excitation laser. The effective resolution was further enhanced by time gating the photon arrival times of the detected fluorescence using a software routine in MATLAB (9). All STED-FCS measurements were performed at the lower, surface attached part of the PM.

Derivation of Eq. 2 of the main text

We will start from Eq. 1 of the main text with only one angular dependence of the fluorescence response for polarized two-photon excitation (i.e. $\theta_0^2=0$, $\theta_0^1=\theta_0$, $A_1=A$) neglecting the background term, F_0. Orientation fluctuation of θ_0 can be modeled by an additive normal distributed component, ε, with zero mean value giving:

$$E\{F(\theta)\}=E\left\{A\cdot\cos(\theta-\theta_0-\varepsilon)^4\right\}=E\left\{A\cdot\left(\frac{3}{8}+\frac{1}{2}\cdot\cos(2\cdot(\theta-\theta_0-\varepsilon))+\frac{1}{8}\cdot\cos(4\cdot(\theta-\theta_0-\varepsilon)\right)\right\} \quad \text{(S5)}$$

Using the relation $\cos(x-y)=\cos(x)\cdot\cos(y)-\sin(x)\cdot\sin(y)$, the right hand side of Eq. S5 can be expanded as Eq. S(6):

$$E\left\{A\cdot\left(\frac{3}{8}+\frac{1}{2}\cdot\cos(2\theta-2\theta)\cdot\cos(2\varepsilon)-\frac{1}{2}\cdot\sin(2\theta-2\theta)\cdot\sin(2\varepsilon)+\frac{1}{8}\cdot\cos(4\theta-4\theta)\cdot\cos(4\varepsilon)-\frac{1}{8}\cdot\sin(4\theta-4\theta)\cdot\sin(4\varepsilon)\right)\right\}$$

The expectation value of a function, $f(\varepsilon)$, is the first moment of the probability density function (PDF), $p(\varepsilon)$, and can be written as:

$$E\{f(\varepsilon)\}=\int_{-\infty}^{+\infty}f(\varepsilon)\cdot p(\varepsilon)d\varepsilon \quad \text{(S7)}$$

The expectation value of the sine function for a Gaussian PDF with zero mean and standard deviation σ is:

$$E\{\sin(\varepsilon)\}=\int_{-\infty}^{+\infty}\sin(\varepsilon)\cdot\frac{1}{\sigma\sqrt{2\pi}}\cdot\exp\left(\frac{-\varepsilon^2}{2\sigma^2}\right)d\varepsilon=0 \quad \text{(S8)}$$

As the integral of an odd function over a symmetric interval is zero, the expectation value of $\sin(\varepsilon)$ is zero as well. Since the cosine function is even, its expectation value is not zero but can be expressed by a Taylor expansion according to

$$E\{\cos(\varepsilon)\}=\int_{-\infty}^{+\infty}\sum_{m=0}^{\infty}\frac{(-1)^m\cdot\varepsilon^{2m}}{(2m)!}\cdot\exp\left(\frac{-\varepsilon^2}{2\sigma^2}\right)d\varepsilon=\sum_{m=0}^{\infty}\frac{(-1)^m}{(2m)!}\int_{-\infty}^{+\infty}\varepsilon^{2m}\cdot\exp\left(\frac{-\varepsilon^2}{2\sigma^2}\right)d\varepsilon \quad \text{(S9)}$$

The integrand on the right hand side comprises the even central moments of the normal distribution which have the values:

$$\int_{-\infty}^{+\infty} \varepsilon^{2m} \cdot \exp\left(\frac{-\varepsilon^2}{2\sigma^2}\right) d\varepsilon = \frac{(2m)!}{2^m \cdot m!} \cdot \sigma^{2m} \tag{S10}$$

Using Eq. S10 in S9 we get:

$$E\{\cos(\varepsilon)\} = \sum_{m=0}^{\infty} \frac{(-1)^m}{(2m)!} \cdot \frac{(2m)!}{2^m \cdot m!} \cdot \sigma^{2m} = \sum_{m=0}^{\infty} \frac{1}{m!} \cdot \left(\frac{-\sigma^2}{2}\right)^m = \exp(-\sigma^2 / m) \tag{S11}$$

Use of Eqs. S8 and S11 in Eq. S6 gives Eq. 2 of the main text.

Simulation of FRAP experiment in the presence of photobleaching during image recording

To illustrate the effect of photobleaching during the recovery process, we set up a FRAP reaction-diffusion simulation in MatLab. Here 150,000 particles were moving by Brownian diffusion with a diffusion constant of $D = 0.1$ μm^2/sec in a square area with a side length of 5 μm and periodic boundaries. Initially, 5 steps of diffusion were simulated in the equilibrated system to determine the number of fluorophores in the ROI pre-bleach. Then all fluorophores in the ROI with radius 1 μm were bleached and the recovery was monitored over 94 additional iterations of Brownian diffusion. During the simulated recovery phase, fluorophores could slowly bleach in the whole field with a given rate constant. For each iteration the number of fluorophores to bleach was calculated as described by Kolin *et al.* (10):

$$N_n^{bleach} = poissrnd\left(N_{n-1} - N_{n-1} \exp\left[-k\Delta t\right]\right), \tag{S12}$$

where n is the number of the current frame, N_{n-1} is the number of fluorescent particles in frame n-1, k is the rate constant for bleaching, Δt is the time between two subsequent images and *poissrnd* is an inherent MatLab function which generates a random number from a Poisson distribution with a given mean. The effect of photobleaching during recovery is shown in Fig. S7A, while Fig. S7B shows the total number of fluorescent particles in the simulated area – including the ROI - as a function of time. From this it can be seen that for moderate bleaching during recovery (green curve, k = 0.001 s^{-1}) the percentage of bleach is reduced while the recovery curve still looks as expected

for a FRAP experiment. This resembles the situation we faced with the two BODIPY-cholesterol's. For stronger bleaching the recovery curve starts to decay after an initial period of recovery (blue and red curves, k = 0.005 s^{-1} and k = 0.01 s^{-1}, respectively). Bleaching during recovery is corrected for by dividing the measured fluorescence recovery curve by the total fluorescence intensity of the imaged area. This is illustrated in Fig. S7C, where the number of fluorophores in the ROI was divided by the total number of fluorophores. This method provided the correct amplitude and half-time of recovery and thereby identical diffusion constants in the simulation.

Synthesis of B-P-Chol

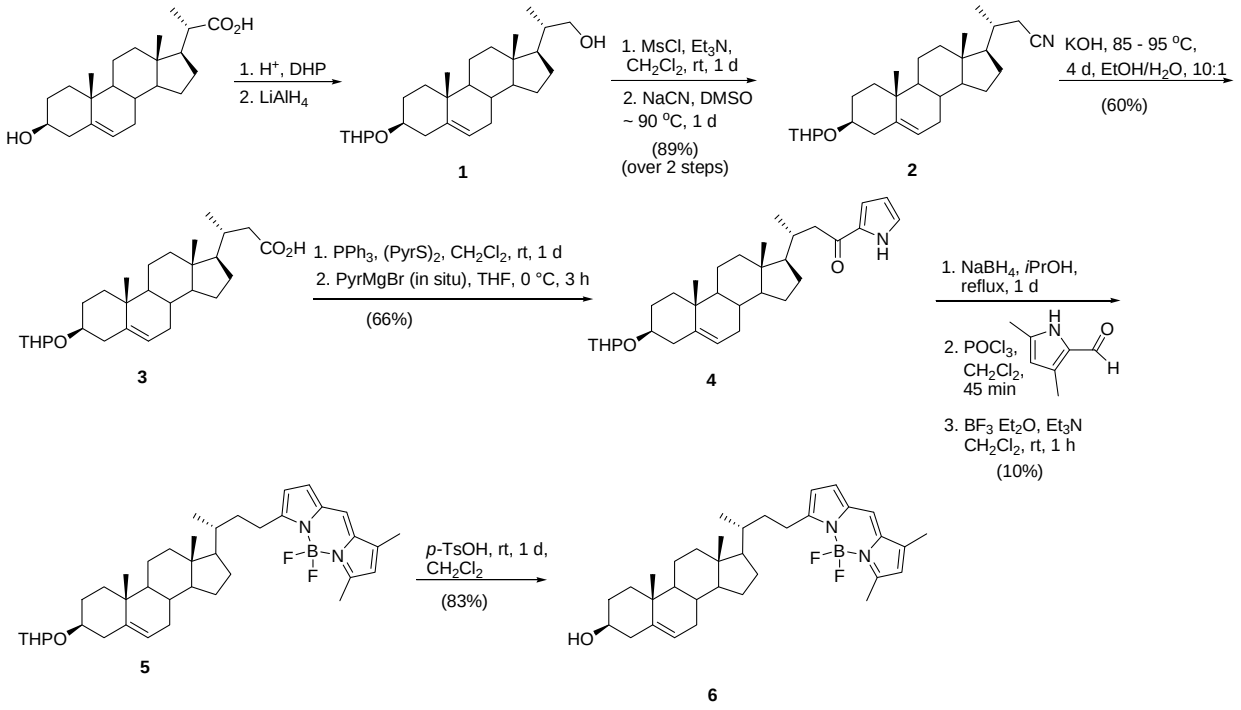

Syntheses of the intermediates and the target probe, B-P-Chol

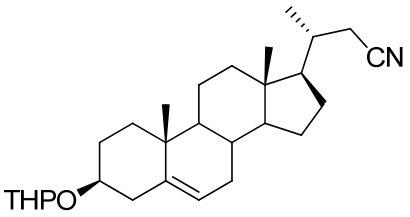

2

Cholesterol derivative **1** (1.40 g, 3.36 mmol) was dissolved in CH_2Cl_2 (30 mL) and subsequently MsCl (1.26 mL, 16.2 mmol) and Et_3N (4.77 mL, 34.2 mmol) were added. The reaction mixture was stirred at rt for 1 d. The solution was washed with H_2O (3 x 20 mL), dried with $MgSO_4$, filtered, and concentrated in vacuo, affording 1.81 g of the crude mesylated cholesterol derivative. No purification was performed. After the crude mesylated cholesterol derivative (1.81 g) was dissolved in DMSO (20 mL), NaCN (360 mg, 7.31 mmol) was added. The reaction mixture was heated to 90 °C and stirred for 1 d. After the mixture was cooled to rt, H_2O (20 mL) was added. The mixture was extracted with Et_2O (3 x 20 mL) and washed with water (30 mL) and brine (30 mL). The crude product was purified by silica gel chromatography (hexane, hexane/EtOAc gradient: 4:1, 2:1, 1:1), providing 990 mg (89%) of compound **2** as a colorless amorphous solid; mp 170 °C; $[\alpha]_D^{25}$ -36.4 (*c* 0.62, $CHCl_3$); ^{1}H NMR (400 MHz, $CDCl_3$): δ 0.70 (s, 3H), 0.89 - 1.31(m, 14H), 1.38 - 2.01 (m, 21H), 2.15 - 2.39 (m, 4H), 3.44 - 3.58 (m, 2H), 3.88 - 3.95 (m, 1H), 4.69 - 4.74 (m, 1H), 5.31 - 5.37 (m, 1H); ^{13}C NMR (101 MHz, $CDCl_3$): δ 12.1, 19.48, 19.51, 19.8, 20.2, 20.3, 21.07, 21.09, 24.3, 25.0, 25.6, 28.1, 28.2, 29.8, 31.1, 31.42, 31.44, 31.94, 31.96, 32.0, 33.7, 36.87, 36.91, 37.3, 37.6, 38.9, 39.5, 40.4, 42.6, 50.08, 50.11, 54.9, 56.6, 63.0, 63.1, 76.08, 76.11, 97.0, 97.2, 119.2, 121.4, 141.0, 141.2. ESI-HRMS: $C_{28}H_{43}NO_2$ calcd. 448.3186 $[M+Na]^+$, found 448.3181.

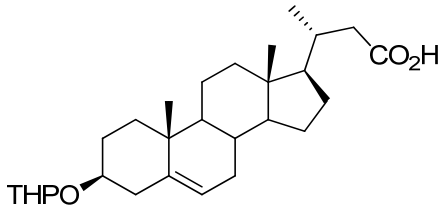

3

Cholesterol nitrile derivative **2** (975 mg, 2.29 mmol) was suspended in EtOH (15 mL). Then a solution of KOH (2.57 g, 45.8 mmol) in H_2O (1.5 mL) was added, and the mixture was heated at reflux for 4 d. After the mixture was cooled to rt, the solvents were evaporated and H_2O (5 mL) was added to the residue. The mixture was extracted with Et_2O (2 x 5 mL). Then the pH was set to 5 - 6 by careful addition of HCl (3 N), and the mixture extracted with CH_2Cl_2 (3 x 5 mL). The combined CH_2Cl_2 layers were dried with $MgSO_4$. Filtration and removal of the solvent in vacuo afforded crude **3** as a yellow oil. The crude product was purified by silica gel chromatography (hexane/EtOAc gradient: 2:1, 1:1, 1:2; EtOAc), giving 611 mg (60%) of compound **3** as an amorphous solid; mp 195 °C; $[\alpha]_D^{25}$ -35.2 (*c* 1.2, $CHCl_3$); ^{1}H NMR (400 MHz, $CDCl_3$): δ 0.71 (s, 3H), 0.85 - 1.35 (m, 14H), 1.38 - 2.06 (m, 20H), 2.14 - 2.38 (m, 2H), 2.47 (dd, *J* = 5.5, 6.2 Hz, 1H), 3.43 - 3.58 (m, 2H), 3.86 - 3.97 (m, 1H), 4.66 - 4.78 (m, 1H), 5.30 - 5.37 (m, 1H); ^{13}C NMR (101 MHz, $CDCl_3$): δ 12.0, 19.5, 19.7, 20.1, 20.2, 21.12, 21.14, 24.3, 25.6, 28.1, 28.4, 31.40, 31.36, 32.0, 33.8, 36.87, 36.91, 37.3, 37.6, 38.9, 39.7, 40.3, 41.4, 42.6, 50.17, 50.21, 55.9, 56.9, 62.9, 63.0, 76.1,

96.9, 97.1, 121.5, 121.6, 141.0, 141.2, 179.6; ESI-HRMS: $C_{28}H_{44}O_4$ calcd. 467.3132 $[M+Na]^+$, found 467.3132.

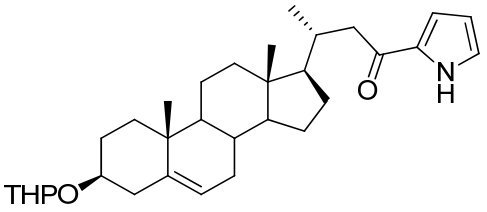

4

PPh_3 (1.69 mmol) and 1,1`-dipyridyl disulfide ($(PyrS)_2$), 1.69 mmol) were dissolved in CH_2Cl_2 (6 mL) and stirred for 15 min. Then a solution of bisnorcholenic acid derivative **3** (577 mg, 1.30 mmol) in CH_2Cl_2 (12 mL) was added, and the reaction mixture was stirred overnight. The solvent was evaporated and the residue was dissolved in THF (10 mL). A solution of MeMgBr (3.71 mL, 5.20 mmol; 1.4 M in toluene/THF) was mixed with THF (5 mL) and cooled to 0 °C. Then pyrrole (469 uL, 6.76 mmol) was added dropwise, and the reaction mixture was stirred for 40 min at 0 °C. A 10-mL solution of the activated ester was added dropwise and the mixture was stirred for an additional 3 h at 0 °C. The solvents were evaporated, the residue was dissolved in CH_2Cl_2 (50 mL), and the solution was cooled to 0 °C and quenched with aqueous saturated NH_4Cl solution (15 mL). The organic layer was separated and the aqueous layer was extracted with CH_2Cl_2 (3 x 15 mL). The combined organic layers were washed with 5% aqueous K_2CO_3 solution (50 mL), H_2O (50 mL), and brine (50 mL), and then dried with $MgSO_4$. Filtration and evaporation of the solvent gave crude pyrrole derivative **4**. Purification by silica gel chromatography (hexane/EtOAc gradient: hexane; 40:1, 20:1, 12:1, 8:1, 4:1) afforded 421 mg (66%) of ketone **4** as a colorless amorphous solid; mp 181 °C $[\alpha]_D^{25}$ -34.4 (*c* 0.47, $CHCl_3$); ^{1}H NMR (500 MHz, $CDCl_3$): δ 0.73 (s, 3H), 0.82 - 1.29 (m, 14H), 1.32 - 1.76 (m, 12H), 1.78 - 2.05 (m, 6H), 2.06 - 2.39 (m, 3H), 2.43 - 2.54 (m, 1H), 2.74 - 2.83 (d, *J* = 14.3 Hz, 1H), 3.43 - 3.58 (m, 2H), 3.87 - 3.96 (m, 1H), 4.71 (s, 1H), 5.34 (m, 1H), 6.26 (s, 1H), 6.89 (s, 1H), 7.01 (s, 1H) 9.68 (s, 1H); ^{13}C NMR (100 MHz, $CDCl_3$): δ 12.0, 19.5, 19.8, 20.1, 20.2, 21.1, 24.4, 25.6, 28.1, 28.7, 29.8, 31.4, 32.0, 34.3, 36.8, 36.9, 37.3, 37.5, 38.9, 39.8, 40.3, 42.7, 45.2, 50.19, 50.23, 56.7, 56.9, 62.9, 63.0, 76.1, 97.0, 97.1, 110.6, 116.3, 121.5, 121.6, 124.6, 133.0, 141.0, 141.2, 191.4; ESI-HRMS: $C_{32}H_{47}NO_3$ calcd. 494.3629 $[M+Na]^+$, found 494.3626.

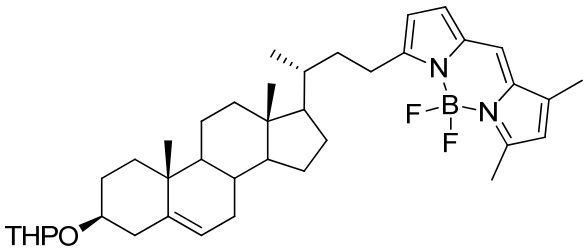

5

To a solution of ketone **4** (10 mg, 0.023 mmol) in *i*-PrOH (1.5 mL) was added $NaBH_4$ (4.5 mg, 0.12 mmol). The reaction mixture was heated at reflux for 1 d. After the mixture was cooled to rt, H_2O (1.5 mL) was added, and the mixture was extracted with CH_2Cl_2. The combined organic layers were washed with H_2O (2 mL) and brine (2 mL). After the organic layer was dried with $MgSO_4$ and filtered, the solvent was removed in vacuo, providing 12 mg of compound **5** as a colorless oil. No purification was performed. The crude product was dissolved in CH_2Cl_2 (2 mL) and 3,5-

dimethylpyrrole carboxaldehyde (25.5 mg, 0.210 mmol) and $POCl_3$ (2.05 μL, 0.021 mmol) were added. The reaction mixture was stirred for 45 min at rt. Then Et_3N (41.0 mL, 0.294 mmol) and $BF_3{\cdot}OEt_2$ (42.5 mL, 0.336 mmol) were added and stirring was continued for 1 h at rt. The solution was washed with H_2O (3 x 1 mL) and dried with $MgSO_4$. After filtration and evaporation, crude BODIPY derivative **5** was isolated as a dark blue oil. The crude product was purified by silica gel chromatography (hexane/EtOAc gradient: hexane; 40:1, 20:1, 12:1, 8:1, 4:1) followed by preparative TLC (hexane/EtOAc 8:1) to afford 1.4 mg (10%) of BODIPY derivative **5** as a red amorphous solid together with some of target compound **6** (which presumably formed when the THP was removed during the NMR spectroscopy of **5** in $CDCl_3$). ^{1}H NMR (500 MHz, $CDCl_3$): δ 0.73 (s, 3H), 0.79 - 1.73 (m, 14H), 1.81 - 1.92 (m, 2H), 1.98 - 2.05 (m, 2H), 2.32 - 2.38 (m, 2H), 2.44 - 2.52 (m, 1H), 2.76 - 2.81 (m, 1H), 3.44 - 3.55 (m, 2H), 3.88 - 3.96 (m, 1H), 4.70 - 4.73 (m, 1H), 5.32 - 5.37 (m, 1H), 6.25 - 6.29 (m, 1H), 6.87 - 6.90 (m, 1H), 6.99 - 7.02 (m, 1H); ESI-HRMS: $C_{39}H_{55}BF_2N_2O_2$ calcd. 633.4397 $[M+H]^+$, found 633.4401. $C_{34}H_{47}BF_2N_2O_2$ calcd. 549.3822 $[M+H]^+$, found 549.3831.

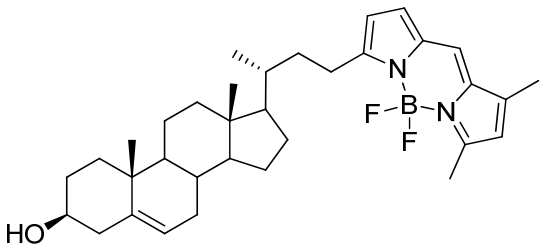

6

BODIPY derivative **5** (1.4 mg, 2.2 μmol) was dissolved in CH_2Cl_2 (0.4 mL) and *p*-TsOH (0.4 mg, 2.2 μmol) was added. The mixture was stirred for 1 d at rt. The solvent was evaporated and the crude product was purified by preparative TLC (hexane/EtOAc 4:1), affording 1 mg (83%) of B-P-Chol (**6**) as a red amorphous solid. ^{1}H NMR (400 MHz, $CDCl_3$): δ 0.67 (s, 3H), 0.76 - 1.69 (m, 14H), 1.78 - 2.03 (m, 11H), 2.22 (s, 3H), 2.23 - 2.30 (m, 2H), 2.31 - 2.35 (m, 1H), 2.54 (s, 3H), 2.95 - 3.02 (m, 1H), 3.47 - 3.54 (m, 1H), 3.60 - 3.64 (m, 1H), 5.34 (m, 1H), 6.06 (s, 1H), 6.25 (d, J = 4.15 Hz, 1H), 6.88 (d, J = 3.85 Hz, 1H), 7.03 - 7.04 (m, 1H); ESI-HRMS: $C_{34}H_{47}BF_2N_2O_2$ calcd. 549.3822 $[M+H]^+$, found 549.3829.

Supporting figures

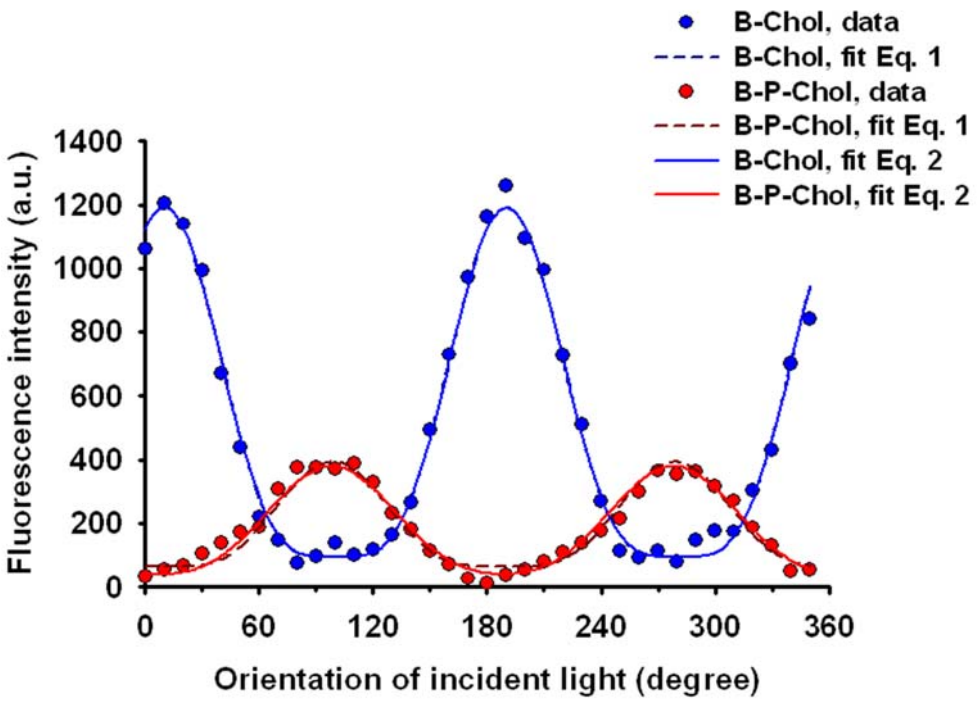

Fig. S1. Non-linear fit of Eqs. 1 and 2 to polarimetry data of BODIPY-cholesterol probes in GUVs. Fluorescence response of B-Chol (blue symbols; data, blue lines, fits) and B-P-Chol (red symbols; data, red lines, fits) in GUVs prepared from POPC and cholesterol (7:3 molar ratio) as a function of the rotation angle of the incident linearly polarized excitation light (compare Fig. 2 in the main text). Fit to Eq. 1 (dashed lines) and Eq. 2 of the main text (straight lines) gave almost indistinguishable results.

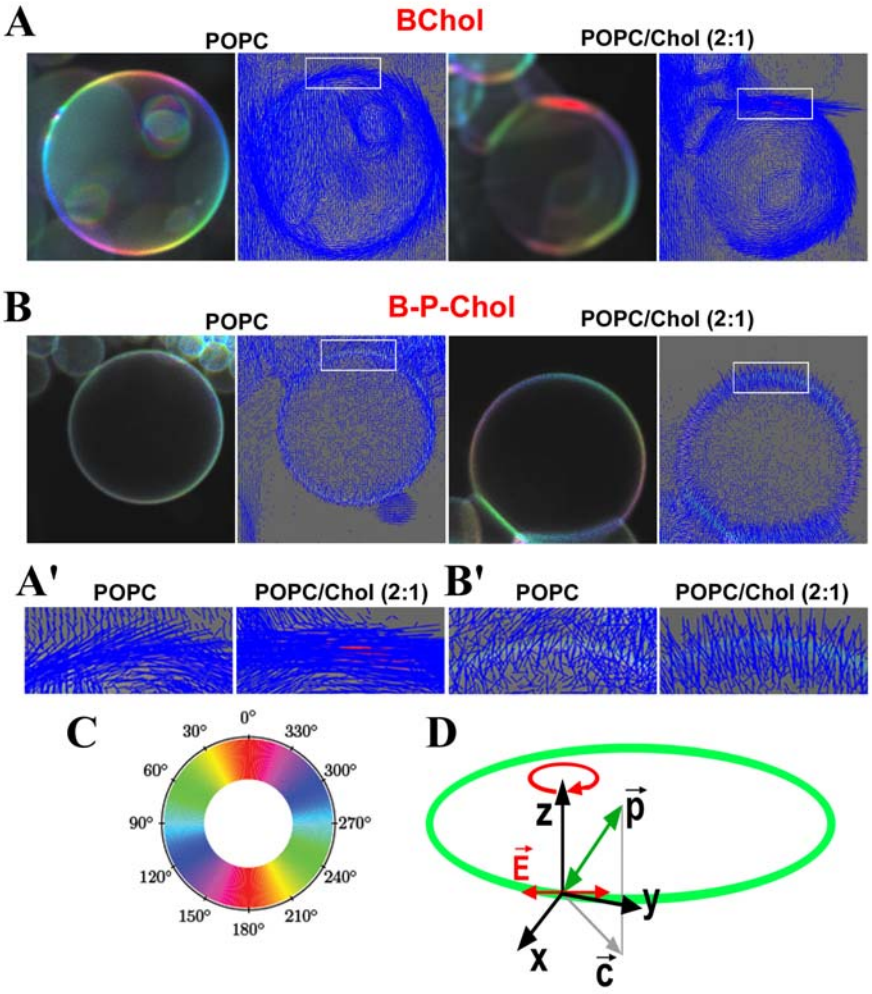

Fig. S2. Pixel-based Fourier analysis of two-photon polarimetry data in model membranes. The fluorescence response of B-Chol (A) and B-P-Chol (B) to the rotating incident field vector, ***E***, was analyzed using a discrete Fourier transform of the pixel intensities. The two left images in panels A and B show the color- and vector-coded representation of the fluorescence response, respectively, for B-Chol and B-P-Chol in GUVs made of POPC only. The two right images of panel A and B show the same analysis for both sterol probes in GUVs made of POPC and cholesterol. The rectangular box highlights a region used for zoom of the vector-coded representation in panels A' and B'. Clearly, the small blue lines are oriented almost parallel to the GUV bilayer for B-Chol (A'), while they align perpendicular to the GUV membranes in the case of B-P-Chol (B'). C, color palette used for color-coding of the angle of fluorescence response relative to the incident field in the HSV color model. D, basis of the vector-coded representation: in the laboratory coordinate system with unit vectors *x*, *y*, *z*, the linearly polarized excitation light vector, ***E***, is given in red, making a full rotation in 10^{o} steps yielding 36 images per recording. The main excitation transition moment of the fluorophores is shown as the vector ***p*** in green. The equatorial plane of the GUV appears as a circle shown in green in the microscope focal plane, while the vector ***p*** can have non-vanishing components out of this plane. Detected is the projection of the transition moment vector ***p*** into the focal plane given by the director ***c*** (grey arrow in panel D).

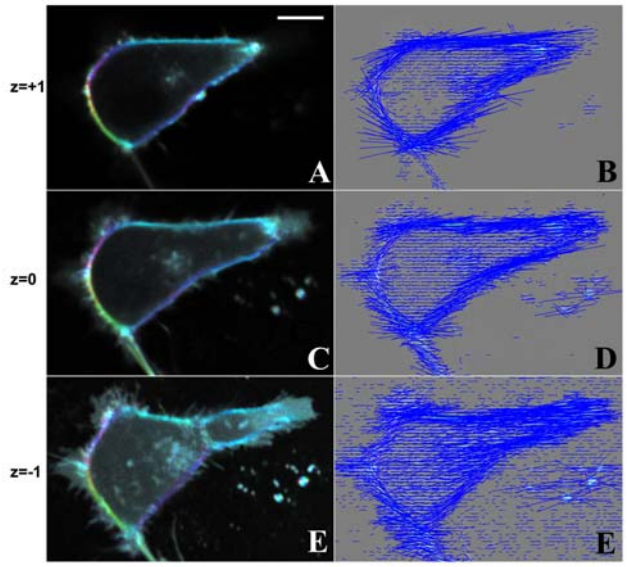

Fig. S3. Two-photon polarimetry of B-Chol in BHK cells at various axial positions. BHK cells were labeled with B-Chol/CD for 1 min, washed with the buffer medium, and imaged on a two-photon microscope with 10^{o} rotation of the incident linearly polarized electric field vector, ***E***. Between recordings of a full rotation consisting of 36 images the focal position was shifted by 1.0 µm downwards in the axial direction starting with a position on the upper half of the cell (A, B; 'z=1') to the cell equator (C, D; 'z=0') and finally to the cell-substrate contact side (E, F; 'z=-1'). The color-coded (A, C, E) and vector-coded (B, D, F) presentation of the fluorescence response is shown. Scale bar = 10 µm.

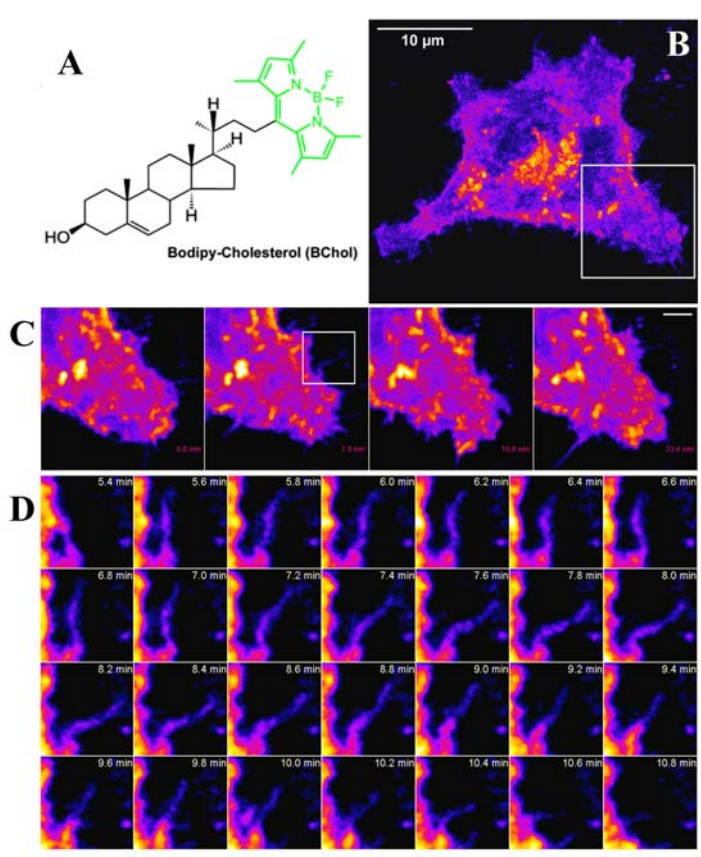

Fig. S4. Two-photon time-lapse imaging of membrane ruffling dynamics in BHK cells. BHK cells were labeled with B-Chol/CD for 1 min, washed with the buffer medium, and imaged on a two-photon microscope for more than 10 min with a frame rate of 0.1 Hz. **A**, B-Chol with the structure of the fluorophore shown in green. B, view of the imaged cell with zoomed box being enlarged in panel C. D, dynamics of the region indicated in the zoom box of panel C. Membrane ruffling and dynamically changing surface protrusions are visible, especially at cell attachment regions. Scale bar in panel C = 1.5 µm.

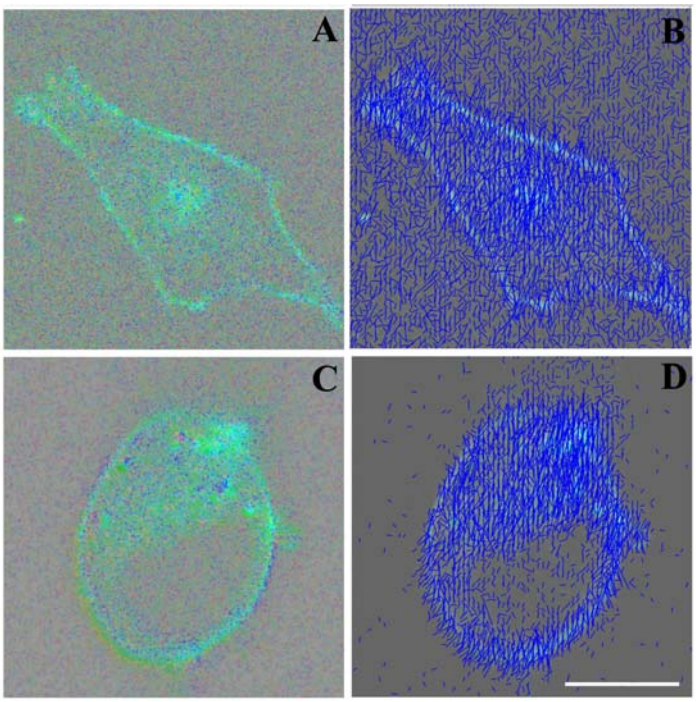

Fig. S5. Two-photon fluorescence polarimetry of B-P-Chol in cell membranes. BHK cells were labeled with B-P-Chol from a B-P-Chol-CD complex as described above. Cells were imaged on a two-photon microscope with 10^{o} rotation of the incident linearly polarized electric field vector, ***E***. The start position of ***E*** is horizontal, as indicated in the legend to Fig. 2B. A, B, show the color-coded (A) and vector-coded (B) presentation of the fluorescence response for intact cells. For C and D, cells were treated with 20 μM cytochalasin for 30 min to disrupt actin. The color-coded (C) and vector-coded (D) presentation of the fluorescence response is shown for a representative cytochalasin-treated cell labeled with B-P-Chol. Scale bar = 15 μm.

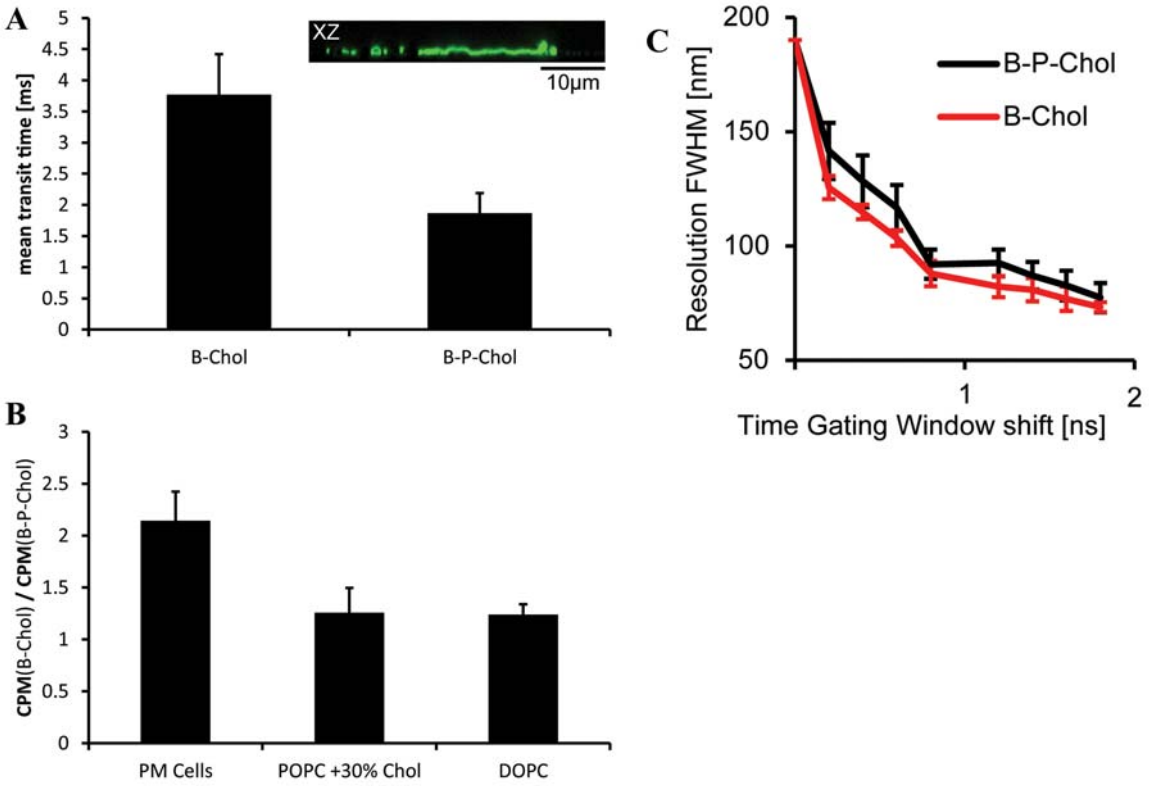

Fig. S6. STED-FCS control experiments

A, Confocal FCS data of B-Chol and B-P-Chol in PM sheets of live Vero cells revealing similar average transit times as measurements in intact Vero cells. Inset: Scanning xz fluorescence image of B-P-Chol in the membrane sheets. B, Ratio of the single-molecule fluorescence brightness (CPM: counts-per-particle) of B-Chol and B-P-Chol in the PM of living Vero cells (PM cells) and in supported lipid bilayers (DOPC: one-component DOPC; POPC + 30% Chol: two-component system POPC and 30 mol% cholesterol) as determined by FCS, demonstrating a 2-fold difference in brightness only for the PM, which is in agreement with the difference in diffusion coefficients. C, Calibration of the STED-FCS measurements: the spatial resolution or full-width-at-half-maximum (FWHM) of the observation spot as determined from the average transit times of the FCS measurements of B-Chol and B-P-Chol in DOPC supported lipid bilayers at 80 mW STED power for different positions of the gated detection (time gating window shift) (44).

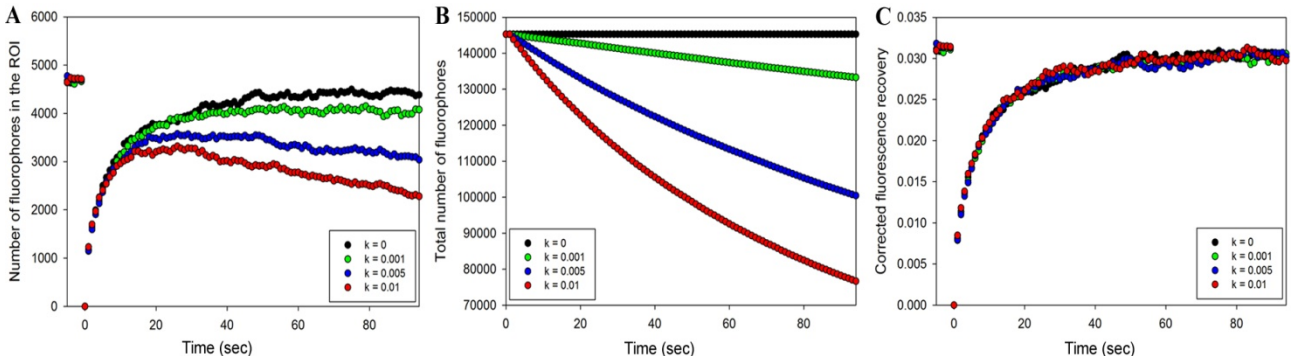

Fig. S7. Normalization of simulated FRAP data to correct for photobleaching during acquisition. A, FRAP curves for simulated experiments with different bleach rates during fluorescence recovery. B, curves of the total number of fluorophores as a function of time for the same bleach rates. C, recovery curves were corrected by dividing the measured recovery curve (A) by the total number of fluorophores (B).

SUPPORTING REFERENCES

1. Wüstner, D., L. M. Solanko, E. Sokol, F. W. Lund, O. Garvik, Z. Li, R. Bittman, T. Korte, and A. Herrmann. 2011. Quantitative Assessment of Sterol Traffic in Living Cells by Dual Labeling with Dehydroergosterol and BODIPY-cholesterol. Chem. Phys. Lipids 164:221-235.
2. Angelova, M. I., S. Soléau, P. Méléard, J. F. Fuaucon, and P. Bothorel. 1992. Preparation of giant vesicles by external AC electric fields. kinetics and applications. Prog. Colloid Polym. Sci. 89:127-131.
3. Bernchou, U., J. Brewer, H. S. Midtiby, J. H. Ipsen, L. A. Bagatolli, and A. C. Simonsen. 2009. Texture of lipid bilayer domains. J. Am. Chem. Soc. 131:14130-14131.
4. Thevenaz, P., U. E. Ruttimann, and E. Unser. 1998. A pyramid approach to subpixel registration based on intensity. IEEE Transactions on Image Processing 7:27-41.
5. Axelrod, D., Koppel, D.E., Schlessinger, J., Elson, E., and Webb, W.W. 1976. Mobility measurement by analysis of fluorescence photobleaching recovery kinetics. Biophys. J. 16:1055-1069.
6. Yguerabide, J., J. A. Schmidt, and E. E. Yguerabide. 1982. Lateral mobility in membranes as detected by fluorescence recovery after photobleaching. Biophys. J. 40:69-75.
7. Mueller, V., C. Ringemann, A. Honigmann, G. Schwarzmann, R. Medda, M. Leutenegger, S. Polyakova, V. N. Belov, S. W. Hell, and C. Eggeling. 2011. STED nanoscopy reveals molecular details of cholesterol- and cytoskeleton-modulated lipid interactions in living cells. Biophys. J. 101:1651-1660.
8. Klar, T. A., S. Jakobs, M. Dyba, A. Egner, and S. W. Hell. 2000. Fluorescence microscopy with diffraction resolution barrier broken by stimulated emission. Proc. Nat. Acad. Sci. U. S. A. 97:8206-8210.
9. Vicidomini, G., G. Moneron, K. Y. Han, V. Westphal, H. Ta, M. Reuss, J. Engelhardt, C. Eggeling, and S. W. Hell. 2011. Sharper low-power STED nanoscopy by time gating. Nat. Methods 8:571-573.
10. Kolin, D. L., S. Costantino, and P. W. Wiseman. 2006. Sampling Effects, Noise, and Photobleaching in Temporal Image Correlation Spectroscopy. Biophysical Journal 90:628-639.